LOW-FREQUENCY OCEAN ACOUSTICS – MEASUREMENTS FROM THE LOFOTEN-VESTERÅLEN OCEAN OBSERVATORY, NORWAY

S Garibbo	Department of Physics, University of Bath, Bath, UK
Ph Blondel	Department of Physics, University of Bath, Bath, UK
G Heald	Defence Science and Technology Laboratory, Porton Down, UK
R Heyburn	AWE Blacknest, Aldermaston, UK
A Hunter	Department of Electronic Engineering, University of Bath, Bath, UK
D Williams	Defence Science and Technology Laboratory, Porton Down, UK

1 INTRODUCTION

Sounds dominate the oceans, spanning all frequencies and coming from different sources: natural (e.g. wind, rain, thermal), biological (e.g. marine mammals, fish) and anthropogenic (e.g. ships, seismic exploration). Very-low frequency hydroacoustic signals ($<$ 100 Hz) are often associated with geophysical processes, like earthquakes and landslides, but they can be linked to man-made activities, like offshore industry or fish blasting. Understanding the mechanisms generating noise below 100 Hz, is important for monitoring underwater explosions and other small events (e.g. submarine accidents) on Comprehensive-Nuclear-Test-Ban Treaty hydrophones and to naval operations such as anti-submarine warfare, where noise can be either or both a source of interference and a source of opportunity. Current understanding of these mechanisms is very limited for noise below 100 Hz and the ocean acoustic phenomena below 10 Hz are rarely studied and even less well understood. Very often, the strong background noise will include several distinct sources, some of which can be very close and others louder but propagating from very large ranges, up to ocean-scale due to low absorption at these frequencies. It is therefore very important to understand the key acoustic signatures of these processes, along with their extreme spatial and temporal variability. The measuring and resolving power of ocean observatories can be harnessed to investigate low-frequency ambient noise over long timescales, in a variety of environmental and background noise conditions.

2 DATA AND PROCESSING

The data presented here are taken from the Lofoten-Vesterålen (LoVe) observatory (Fig. 1), which is located approximately 15 km offshore of the Lofoten Islands, at a depth of 255 m on the continental shelf[27]. It is situated within the Hola Trough – one of many troughs formed during the last glaciation – and hosts cold water coral reefs, sandwave fields, and glacigenic deposits[30,32,5]. The hydrophone (a calibrated Ocean Sonic SB35 ETH) records between 10 Hz and 200 kHz, and is mounted approximately 0.5 m above the seabed on a metallic structure anchored into the sea floor[24].

The data were analysed using the Matlab implementation of PAMGuide, which performs calibrated signal processing on passive acoustic data in both terrestrial and aquatic environments[23]. The calibration parameters were taken from the Ocean Sonic hydrophone specifications[24], and compared to previous work using data from the LoVe observatory[27].

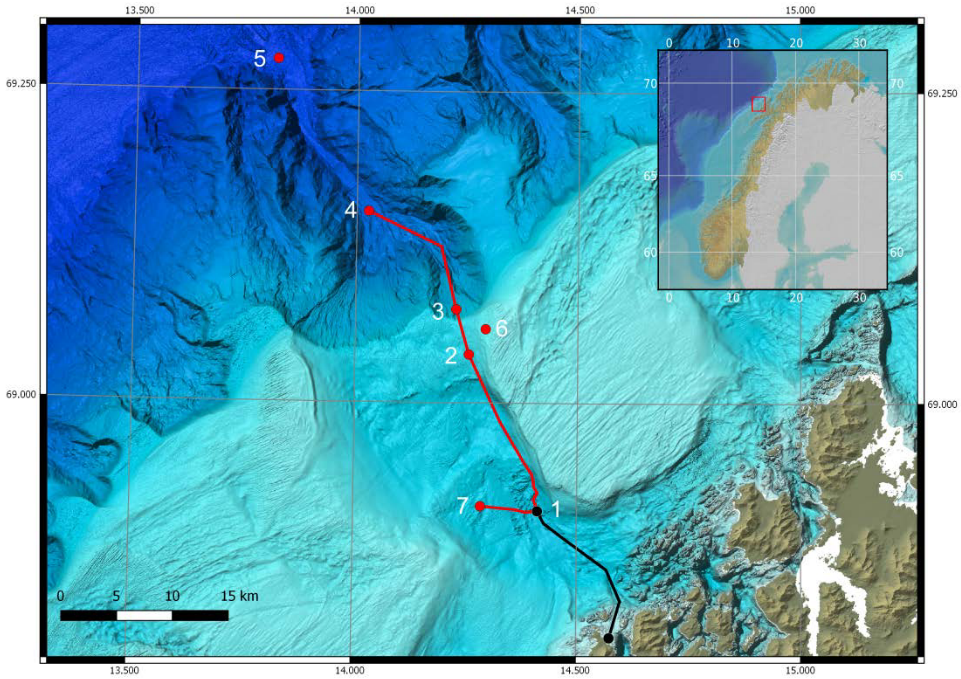

Figure 1: Layout of LoVe observatory offshore of the Lofoten Islands (insert shows the location offshore northern Norway, marked with a red box); numbers 1 to 7 are used to label hydrophone nodes[27].

OBSERVATIONS

Whale vocalisations

The most commonly found whale vocalisation in the LoVe dataset is attributed to fin whales, and is known as the "20 Hz call"[28,7]. The global distribution of fin whales mean that this high amplitude, and long-propagating call is a common feature of the world's ocean soundscape[25]. It is thought to be made by male fin whales during the breeding season to attract females from great distances[25,2] as unlike other whales, fin whales do not gather in specific areas to mate[11].

20 Hz calls are approximately 1 s in duration, consist of a frequency down-sweep between approximately 25 Hz and 17 Hz[25], and are separated by an interval between 9 s and 34 s[7]. This is sometimes accompanied by a higher frequency up-sweep of variable bandwidth. Two groups of higher frequency vocalisations are seen in the LoVe data – one that appears between 40 Hz and 80 Hz, and another that appears between approximately 80 Hz and somewhere upward of 125 Hz, which could suggest that these are recordings of two different pods.

Shipping

Shipping noise is generally acknowledged to be one of the two largest contributors to sound in the ocean under 1,000 Hz[14,34]. Accordingly, shipping noise is observed on every day of available data from the LoVe observatory, ranging from continuous shipping noise over the course of a day, to short blips of shipping noise only minutes in duration. The abundance of shipping noise is most likely due to activity along a main shipping lane, located approximately 55 km northwest of the LoVe observatory, as well as important local shipping traffic in the form of ferries and fishing vessels.

The most distinguishable feature of shipping noise on a spectrogram is bold, horizontal tonal lines. These are attributed to propeller blade cavitation[22] and also internal mechanisms like the engine, pumps and generators[33]. The frequencies at which shipping noise dominates depends on vessel type, load, speed, and also aspects like propeller type and hull design[22].

Another common feature of shipping noise is an upward 'U' pattern[1,33,36]. This is Lloyd's Mirror Effect (LME) – the result of interference between the direct and indirect sound propagation paths as the source point moves. The significance of this pattern is that it can be used, in conjunction with the tonal lines, to trace the source of the shipping noise[36,37], and that the minima of these patterns represents the Closest Point of Approach (CPA) to the hydrophone[38].

Wind

Weather generates and influences sound in the ocean through several mechanisms – such as wave formation, radiative heat transfer, the formation of sea ice etc.[35]. For frequencies below 500 Hz, wind largely generates noise by forcing the surface of the ocean, leading to the formation of surface gravity waves[35,21]. The interactions between surface waves travelling in different directions generate sound at twice the frequency of the surface wave, but only leads to insonification of the far-field if the surface waves have wave numbers of similar magnitude and are travelling in near-opposite directions, creating standing waves[8]. Over the entire year 2018, there were 33 manually-found instances of "white-out" of the spectrograms, where all frequencies between 10 Hz and 125 Hz were saturated. These instances all coincided with periods of higher wind speeds or local storms, but not all periods of high wind speeds coincided with a period of higher broadband noise.

Earthquakes

Another common signal in the LoVe dataset comes from earthquakes. For example, on 25^{th} April 2018, the International Seismological Centre (ISC) bulletin recorded an earthquake at 00:05:06 UTC of magnitude (m_b) 3.4, and another earthquake at 00:06:56 UTC of magnitude (m_b) 4.9[19]. The epicenters for both earthquakes were approximately 88 km southeast of Jan Mayen, 830 km away from the LoVe observatory. Assuming the speed of sound through seawater is 1500 m.s^{-1}, an approximate travel time through the water column would be 9.2 minutes, giving a predicted arrival time of 00:16:08 UTC for the larger of the two earthquakes. The observed signal at 00:16:10 UTC arrives within 0.5% of the predicted travel time. In addition to the sound that travels through the water (also known at the T-phase), seismic waves generated by the earthquake propagate through the solid Earth and are also detected by the LoVe hydrophone. Multiple signals can therefore be detected from a single earthquake at the hydrophone. Hydrophones commonly detect P-waves and teleseismic waves from earthquakes[13,31,3], and in total, 62 seismic events were found in the LoVe data in 2018.

ANALYSIS

Wind

Periods of high wind speeds near the LoVe observatory sometimes coincide with a "white-out" of the spectrogram, and other times, there is no signal to be seen, and no increase in broadband sound pressure level – as can be seen in Fig. 2). For example, from 6^{th} to 7^{th} January (Fig. 2, upper far left panel), the wind blew in a NNE direction, rising by 5 m.s^{-1} over the 24-hour period. This coincided with a 7 dB increase in broadband SPL. Comparatively, during the 24-hour period of 12^{th} to 13^{th} May (Fig. 2, lower far left panel), the wind also blew in a NNE direction, rising by 1.83 m.s^{-1} and coinciding with a 2.9 dB increase in broadband SPL. Wind speed alone can only be used to crudely estimate the amount of noise transmitted underwater, as factors like duration of wind, fetch,

constancy, and its direction in relation to local swells and currents, and nearby topography[34,9] are also important. Previous work done in other areas of shallow water suggests that a wind speed threshold of approximately 10 m.s^{-1} generally has to be exceeded to cause significant changes in mean sound levels[17], but there is also a strong site-dependence for wind-driven noise, depending on factors like ocean bottom properties, water depth, and sound-speed profiles[18,29].

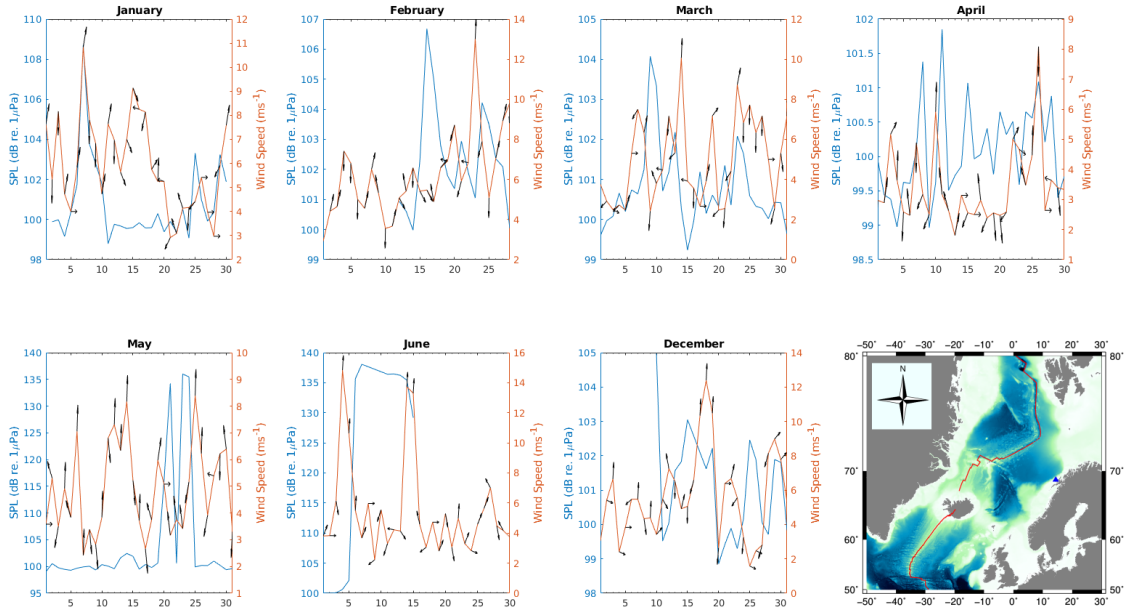

Figure 2: Acoustic effects of wind direction, indicated by tiny arrows. Lower far right panel shows the location of the LoVe hydrophone (blue triangle) and the larger surrounding area. All other panels shows the broadband SPL (blue), wind speed (red), and wind direction (black arrows), recorded for each day of a different month [upper: January, February, March, April; lower: May, June, December].

Earthquakes

An arbitrary area was selected around the LoVe observatory primarily to minimise the size of the ISC earthquake bulletin to be manually checked against the LoVe data to 1,090 earthquakes, from what would have been hundreds of thousands. The area was also selected as it included a variety of potential geophysical acoustic sources – for example, glaciers in Greenland and Svalbard, the Mid-Atlantic Ridge, and volcanic activity in Iceland.

An earthquake was considered detected if the signal appeared in the LoVe data within $\pm 10\%$ of the predicted travel time. For the seismic arrivals, this reflected a reasonable variance in travel time residuals for the area[20]. Travel-times of acoustic waves in the water were calculated using the source-to-station distance and a velocity of 1500 m.s^{-1}. The open-source software TauP[12] was used as a seismic phase travel time calculator. The required input parameters for the calculation included the geodesic distance between the earthquake epicentre and the LoVe hydrophone, and the earthquake source depth. The source depth was chosen as a fixed 0 km as much of the depth data is not reported in the ISC[19] database, and changing the depth by up to 10 km at a time impacts resulting arrival time predictions by less than one second, which would be highly unlikely to cause the prediction to fall outside of the 10% error window. Locations of the 62 earthquakes that were detected in 2018 are

shown in Fig. 3. The detected earthquake magnitudes (m_b) ranged between 2.5 and 4.9, at source-to-station distances ranging from 73 km to 2212 km. 56% of the 1090 earthquakes from the ISC bulletin fell within periods when the hydrophone was not recording, and a further 29% of ISC events did not have any corresponding signal at the LoVe observatory. Approximately 20% of the remaining earthquakes were detected at the LoVe observatory either as single arrival events, or multiple arrival events, but outside of the 10% error window, leaving 5% of the arrivals falling within the error window. Although not discussed here, an additional seismic bulletin[26] that contains earthquakes of magnitudes down to -1.98 has been collected, and the signals that fall outside of the error window will be cross-referenced.

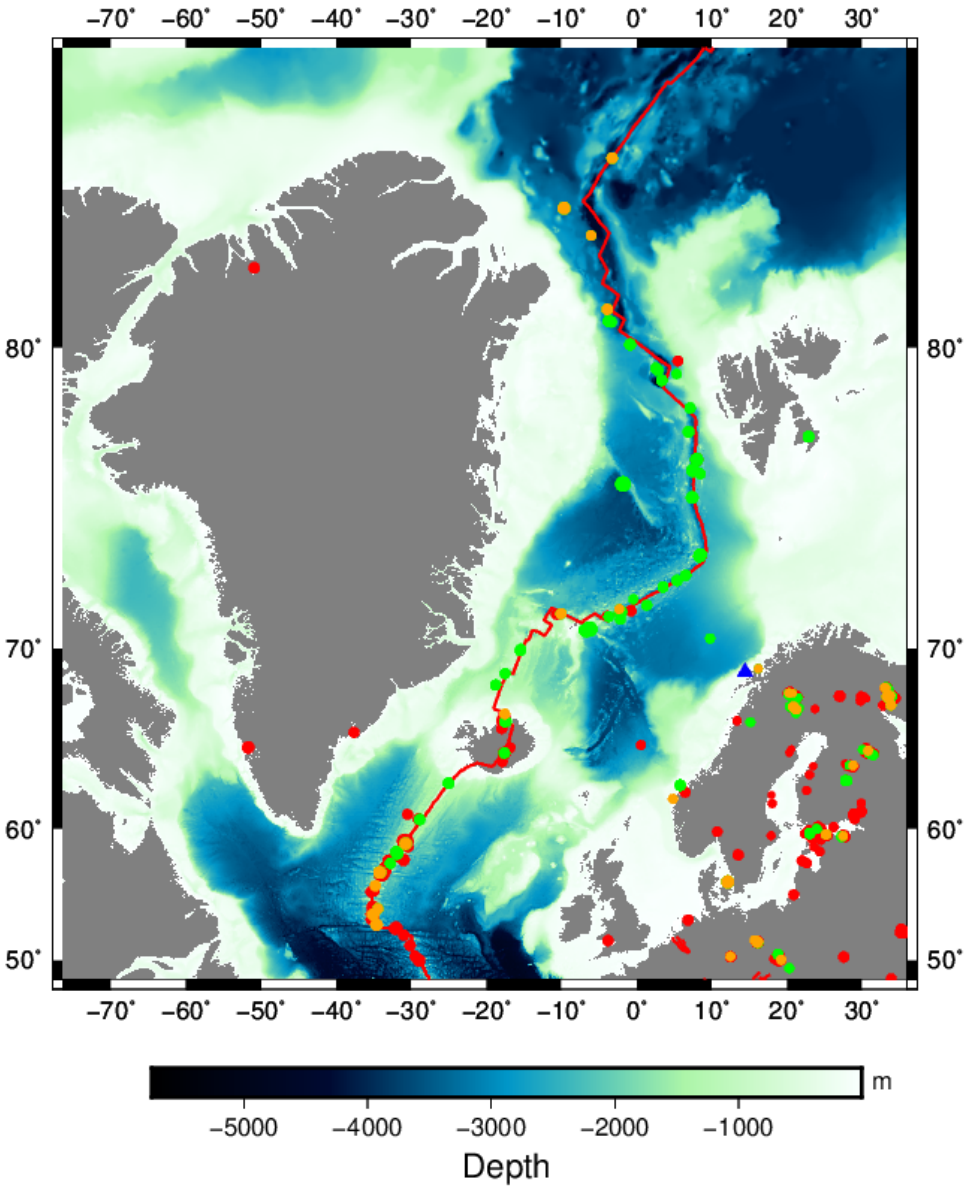

Figure 3: Distribution of detected and undetected earthquakes from the LoVe observatory. Green spots represent earthquakes with multiple corresponding arrivals in the LoVe data, orange spots represent single arrivals, and red spots have no corresponding arrival. The earthquake spots are scaled so that larger magnitude earthquakes are represented by larger diameter spots. The red line represents the Mid-Atlantic Ridge, and the bathymetry data is from GEBCO[15].

Possible reasons that some earthquakes were detected whilst others, especially if from similar locations were not, could involve different earthquake magnitudes, different paths of propagation, and the ambient noise levels at the LoVe observatory. The acoustic signal of earthquakes of a magnitude of 2 or less are unlikely to propagate as far as a larger magnitude earthquake[31], and the propagation paths from some geological regions may mean that a signal is less likely to reach the LoVe observatory. For example, the region of the Mid-Atlantic Ridge to the south of Iceland appears to be a location from which an earthquake signal rarely appears at the LoVe observatory. As can be seen in the bathymetry of Fig. 3, this coincides with two large fracture zones – the Charlie-Gibbs and the Bight Fracture Zones. Fractured rock delays acoustic propagation and reduces signal amplitude[4], so it is unsurprising that the earthquakes from this geological setting mostly went undetected at the LoVe observatory. Other possible explanations for undetected events could involve the bathymetry between the epicentre and the observatory – for example, in Fig. 3 a bathymetric high (the Rockall Rise) is visible to the northwest of the U.K., and presents a possible barrier to some events originating south of Iceland. Particularly, sediment properties, depth of the source, and bathymetric slope are known to have significant impacts on the acoustic signature characteristics of the water arrival (or T-phase)[6] – but to properly determine these effects, thorough testing of propagation models would be necessary. Other explanations for undetected earthquakes at the LoVe observatory include a rise in local ambient noise, as a result of a storm for instance, or that the arrival coincides with a masking transient noise at the LoVe observatory like shipping.

CONCLUSION

In the LoVe dataset daily shipping signals were found, with insightful features like LME interference patterns, which can be used to determine CPA, and even track vessel movements[36,37]. Wind signals were found – with spectrum saturation occurring during periods of high wind speed. There were also instances where wind speed and broadband SPL (see Figure 2) showed no correlation at all. It was concluded that broadband SPL was too crude a measurement of wind speed, and that factors like fetch, constancy of wind, direction in relation to currents, swells, and nearby topography should also be taken into account[34,9]. The most common biological source identified in the LoVe data was from fin whales – specifically the “20 Hz call” male fin whales make during breeding season. Strong seasonal variation in whale vocalisations was observed, with the 20 Hz call peaking in occurrence during the winter months (breeding season), and the higher frequency calls were more commonly observed in spring. 62 earthquakes were verified by their seismic and water phases, with epicentres ranging as far as 2212 km away from the LoVe observatory. Possible reasons for unverified events include geological setting (earthquakes originating from a transfer zone are less likely to propagate as efficiently), bathymetry that results in a propagation path of high transmission loss, that the arrivals coincided with periods of high ambient noise, like wind, or a high transient noise, like shipping, or that the manually-found signals actually correspond to more local, lower magnitude events.

ACKNOWLEDGEMENTS

This research is supported by the UK Engineering and Physical Sciences Research Council (EPSRC), as part of industrial Cooperative Award in Science and Technology (iCASE) project #2279119, supported by Defence Science & Technology Laboratory (Dstl) and AWE Blacknest.

REFERENCES

1. C. Audoly, V. Meyer, “Measurement of radiated noise from surface ships - Influence of the sea surface reflection coefficient on the Lloyd’s mirror effect”,

Proceedings of ACOUSTICS 2017 Perth: Sound, Science and Society, **Section 3**, 1–10 (2017).

2. M. G. Aulich, R. D. McCauley, D. Robert, B.J. Saunders, M.J.G. Parsons, “Fin whale (Balaenoptera physalus) migration in Australian waters using passive acoustic monitoring”, *Nature Scientific Reports*, **9**, 1–12 (2019).
3. D. K. Blackman, C. E. Nishimura, J. A. Orcutt, “Seismoacoustic recordings of a spreading episode on the Mohns Ridge”, *Journal of Geophysical Research: Solid Earth*, **105:B5**, 10961–10973 (2000).
4. F. K. Boadu, L. T. Long, “Effects of fractures on seismic-wave velocity and attenuation”, *Geophysical Journal International*, **12:1**, 86-110 (1996).
5. R. Bøe, V. K. Bellec, M. F. J. Dolan, P. Buhl-Mortensen, L. Buhl-Mortensen, D. Slagstad, L. Rise, “Giant sandwaves in the Hola glacial trough off Vesterålen, North Norway”, *Marine Geology* **267:1**, 36–54 (2009).
6. A. Bottero, “Full-wave numerical simulation of T-waves and of moving acoustic sources”. **PhD Thesis**, *Aix Marseille Université*, (2019).
7. S. J. Buchan, L. Gutierrez, N. Balcazar-Cabrera, K. M. Stafford, “Seasonal occurrence of fin whale song off Juan Fernandez, Chile”, *Endangered Species Research*, **39:1998**, 135–145 (2019).
8. D. H. Cato, “Theoretical and measured underwater noise from surface wave orbital motion”, *Journal of the Acoustical Society of America*, **89:3**, 1096–1112 (1991).
9. P. Cauchy, K. J. Heywood, N. D. Merchant, B. Y. Queste, P. Testor, “Wind speed measured from underwater gliders using passive acoustics”, *Journal of Atmospheric and Oceanic Technology*, **35:12**, 2305–2321 (2018).
10. P. A. Ching, D. E. Weston, “Wideband studies of shallow-water acoustic attenuation due to fish”, *Journal of Sound and Vibration*, **18:4**, 499-510 (1971).
11. D. A. Croll, C. W. Clark, A. Acevedo, B. Tershy, S. Flores, J. Gedamke, J. Urban, “Only male fin whales sing loud songs”, *Nature*, **417:6891**, 809–809 (2002).
12. H. P. Crotwell, T. J. Owens, J. Ritsema, “The TauP Toolkit: Flexible seismic travel-time and ray-path utilities”, *Seismological Research Letters*, **70**, 154-160 (1999).
13. R. P. Dziak, D. R. Bohnenstiehl, H. Matsumoto, C. G. Fox, D. K. Smith, M. Tolstoy, T. K. Lau, J. H. Haxel, M. J. Fowler, “P- and T-wave detection thresholds, Pn velocity estimate, and detection of lower mantle and core P-waves on ocean sound-channel hydrophones at the Mid-Atlantic Ridge”, *Bulletin of the Seismological Society of America*, **94:2**, 665–677 (2004).
14. A. Farcas, C. F. Powell, K. L. Brookes, N. D. Merchant, “Validated shipping noise maps of the Northeast Atlantic”, *Science of the Total Environment*, **735**, 139509 (2020).
15. IOC, IHO and BODC, 2003, ”Centenary Edition of the GEBCO Digital Atlas”, published on CD-ROM on behalf of the Intergovernmental Oceanographic Commission and the International Hydrographic Organization as part of the General Bathymetric Chart of the Oceans; British Oceanographic Data Centre, Liverpool
16. O. R. Godø, S. Johnsen, T. Torkelsen, “The LoVe ocean observatory is in operation”, *Marine Technology Society Journal* **48:2**, 24–30 (2014).
17. J. H. Haxel, R. P. Dziak, P. Robert, H. Matsumoto, “Observations of shallow water marine ambient sound: The low frequency underwater soundscape of the central Oregon coast”, *The Journal of the Acoustical Society of America*, **133:5**, 2586-2596 (2013).
18. F. Ingenito, S. N. Wolf, “Site dependence of wind-dominated ambient noise in shallow water”, *Journal of the Acoustical Society of America*, **85:1**, 141-145 (1989).
19. International Seismological Centre, Online Bulletin, https://doi.org/10.31905/D808B830 (2020).
20. A. L. Levshin, J. Scweitzer, C. Weidle, N. M. Shapiro, M. H. Ritzwoller, “Surface wave tomography of the Barents Sea and surrounding regions”, *Geophysical Journal International*, **170:1**, 441-459 (2007).
21. M. S. Longuet-Higgins, “A Theory of the Origin of Microseisms”, *Philosophical Transactions of the Royal Society of London*, **243:857**, 2–35 (1950).
22. M. F. McKenna, D. Ross, S. M. Wiggins, J. A. Hildebrand, “Underwater radiated noise from modern commercial ships”, *The Journal of the Acoustical Society of America*, **131**, 92–103

(2012).
23. N. D. Merchant, K. M. Fristrup, M. P. Johnson, P. L. Tyack, M. J. Witt, P. Blondel, S. E. Parks, "Measuring Acoustic Habitats", *Methods in Ecology and Evolution*, **2041-210X.12330** (2015).
24. METAS, "Ocean Observatory Vesterålen" [online], https://love.statoil.com/Documentation?version=0, (2014), Accessed on: 07-10-2019
25. J. L. Morano, D. P. Salisbury, A. N. Rice, K. L. Conklin, K. L. Falk, C. W. Clark, "Seasonal and geographical patterns of fin whale song in the western North Atlantic Ocean", *The Journal of the Acoustical Society of America*, **132:2**, 1207–1212 (2012).
26. NORSAR, "Seismic Bulletins", https://www.norsar.no/seismic-bulletins/, (2020), Accessed on: 23-05-2020.
27. L. Ødegaard, G. Pedersen, E. Johnsen, "Underwater Noise from Wind at the High North LoVe Ocean Observatory", *UACE 2019 Conference Proceedings*, 359–366 (2019).
28. A. Pereira, D. Harris, P. Tyack, L. Matias, "Lloyd's mirror effect in fin whale calls and its use to infer the depth of vocalizing animals", *Proceedings of Meetings on Acoustics*, **27**, 070002, (2016).
29. C. L. Piggott, "Ambient Sea Noise at Low Frequencies in Shallow Water of the Scotian Shelf", *The Journal of the Acoustical Society of America*, **36:11**, 2152-2163 (1964).
30. S. Sauer, A. Crémière, J. Knies, A. Lepland, D. Sahy, T. Martma, S. R. Noble, J. Schönenberger, M. Klug, C.J. Schubert, "U-Th chronology and formation controls of methane-derived authigenic carbonates from the Hola trough seep area, northern Norway", *Chemical Geology* **470**, 164–179 (2017).
31. P. D. Slack, C. G. Fox, R. P. Dziak, "P wave detection thresholds, Pn velocity estimates, and T wave location uncertainty from oceanic hydrophones", *Journal of Geophysical Research: Solid Earth*, **104:B6**, 13061–13072 (1999).
32. T. Van England, O. R. Godø, E. Johnsen, G. C. A. Duineveld, D. van Oevelen, "Cabled ocean observatory data reveal food supply mechanisms to a cold-water coral reef",*Progress in Oceanography*, **172**, 51–64 (2019).
33. S. C. Wales, R. M. Heitmeyer, "An ensemble source spectra model for merchant ship-radiated noise", *The Journal of the Acoustical Society of America*, **111:3**, 1211–1231 (2002).
34. G. M. Wenz, "Acoustic ambient noise in the ocean: spectra and sources", *The Journal of the Acoustical Society of America*, **34:12**, 1936–1956 (1962).
35. W. S. D. Wilcock, K. M. Stafford, R. K. Andrew, R. I. Odom, "Sounds in the Ocean at 1—100 Hz", *Annual Review of Marine Science*, **6**, 117–140 (2014).
36. M. J. Wilmut, N. R. Chapman, G. J. Heard, G. R. Ebbeson, "Inversion of Lloyd mirror field for determining a source's track", *IEEE Journal of Oceanic Engineering*, **32:4**, 940–947 (2007).
37. J. K. Wilson, "Maritime Surveillance Using a Wideband Hydrophone", *Naval Postgraduate School, Monterey, California* (2007).
38. G. Zhang, T. N. Forland, E. Johnsen, G. Pedersen, H. Dong, "Measurements of underwater noise radiated by commercial ships at a cabled ocean observatory", *Marine Pollution Bulletin*, **153**, 110948 (2020).